ELSEVIER

Chemical Engineering Journal 117 (2006) 231–238

Chemical Engineering Journal

www.elsevier.com/locate/cej

A theoretical model for calculating pressure drop in the cone area of light dispersion hydrocyclones

Qing-Guo Zhao *, Guo-Dong Xia

Key Laboratory of Enhanced Heat Transfer and Energy Conservation, Ministry of Education, College of Environmental and Energy Engineering, Beijing University of Technology, 100 PIN LE YUAN, Chaoyang District, Beijing 100022, PR China

Received 29 August 2005; received in revised form 7 November 2005; accepted 17 November 2005

Abstract

Pressure drop in a hydrocyclone reflects the energy necessary for a separation process. It is very important to predict pressure drop in a hydrocyclone design. In this paper, pressure drop in a light dispersion hydrocyclone is conceptually divided into two parts: dissipated pressure drop and effective pressure drop. The latter is the pressure drop in the major separation region that represents the energy converted from static to kinetic form. Based on velocity distributions established by ZHAO and MA, a theoretical model is developed to calculate effective pressure drop in the cone region of light dispersion hydrocyclones. Experimental results prove that the model can give a very good prediction of effective pressure drop. Though the calculated results are more or less higher than the measured, their differences are small enough to be neglected in a hydrocyclone design practice. It is indicated that effective pressure drop can be correlated to flowrate by $\Delta p_{BC} = -0.000816 - 0.00186Q + 0.00667Q^2$ in the range of $Q = 1$–$5\ m^3/h$ at $F = 6\%$ and $R_o = 4$ mm for 30 mm hydrocyclone with cycloid and involute inlets. Increase of split ratio is shown to lead to decrease of effective pressure drop, while overflow orifice diameter affects the effective pressure drop in a reverse manner. According to the model developed in present paper, it is possible to study influences of operating conditions, design parameters and fluid properties on effective pressure drop.

Keywords: Hydrocyclone; Pressure drop; Theoretical model; Effective pressure drop

1. Introduction

Since the pioneering work [1–3] made by Thew's group on deoily hydrocyclones (generally called light dispersion hydrocyclone), this kind of highly-efficient separating device has been rapidly industrialized, especially for offshore oil production process [4–9]. The basic characteristic is the migration probability, which represents the separation efficiency of a hydrocyclone versus dispersed droplet size, and has been well correlated by Thew and his co-workers [3–5]. Another important characteristic is the pressure drop, which is representative of the driving energy necessary for a certain separation. The latter was also experimentally correlated to Reynolds number and inlet size by Thew [5] for Thew type hydrocyclones with involute inlets. Generally speaking, the overall pressure drop in Thew type hydrocyclone can be calculated according to Thew's correlation, which will not be available for hydrocyclones different from that of Thew type. In addition, it is often of academic importance to know effects of design parameters on pressure drop if optimization is to be taken into account. Nowadays, treatment of waste water, removal of printing ink from paper pulp made of waste paper, separation of oil from orange juice, removal of grease from milk, etc. are all potential applications of light dispersion hydrocyclones. Often dispersed droplets in these processes are of very small size, say, order of ten micron. In these cases, the separation will be difficult. It is well know that separation capacity increases with decrease of hydrocyclone size. So it is possible to separate small dispersed droplets by decreasing hydrocyclone size, but the pressure drop will be enhanced. From these backgrounds the significance of research of hydrocyclone pressure drop can be viewed from two aspects. One is its presentation of energy consumption for separation, and the other is its competitive feature against separation capacity (that is, small pressure drop means large room of improving separation efficiency).

* Corresponding author. Tel.: +86 10 67396661x8319; fax: +86 10 67392774.
E-mail addresses: zhaoqg@yahoo.com.cn, zhaoqingguo@bjut.edu.cn (Q.-G. Zhao).

1385-8947/$ – see front matter © 2006 Elsevier B.V. All rights reserved.
doi:10.1016/j.cej.2005.11.012

Due to the complex of fluid flow in hydrocyclones, studies on pressure drop have been experimentally carried out [5] in past years. When a hydrocyclone is designed in a different way from Thew's type, new method must be developed to predict its pressure drop. Martins et al. [10] derived a theoretical relationship with coefficient and exponential index fitted from experimental data, but effects of design parameters were not covered in it. It seems that it is necessary to develop a stringent theoretical algorithm for predicting the influence of design parameters on pressure drop.

In a solid–liquid hydrocyclone, pressure drop is normally referred to as the difference between inlet pressure and that in the point immediately after overflow exit. This definition is convenient due to the predominance of overflow rate over the underflow rate and the fact that the overflow in many applications remains the process stream. In a light dispersion hydrocyclone, however, most of the fluid leaves hydrocyclone through underflow and the pressure drop from entry to underflow defines the major energy necessary for separation. The present concern focuses on the development of theoretical model for calculating entry-underflow pressure drop.

In this paper, the pressure drop of a hydrocyclone is conceptually divided into two parts. One is called "dissipated pressure drop", corresponding to the pressure drop from entry 1 to the point 2 joining cylindrical and conical section, as shown in Fig. 1. It is the energy consumption due to the expansion of fluid flow channel, abrupt turn of fluid flow and fluid friction. The second part is called "effective pressure drop", that is, the pressure drop from point 2 to point 3 (joining conical section and tail section) shown in Fig. 1. It is deemed that separation happens in the two conical sections, and that the cylindrical section only serves to make a transition of fluid flow from linear movement at entry to axially symmetrical flow in conical section [4,11]. The effective pressure drop thus represents the effective energy for separation, that is, the energy for conversion from static energy to kinetic energy. The objective of this paper is to develop a theoretical model to calculate effective pressure drop of light dispersion hydrocyclones.

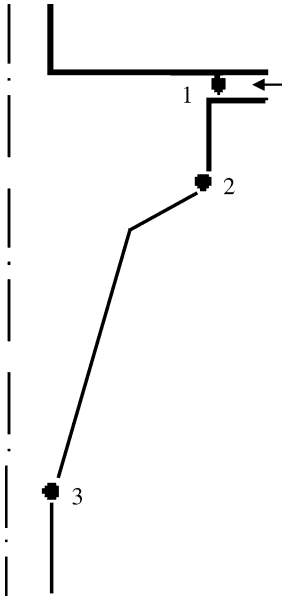

Fig. 1. points for defining two kinds of pressure drop.

2. Theory

2.1. Velocity distributions

It is important to know tangential velocity distributions in a hydrocyclone for calculating pressure drop. Much work has been done on velocity distributions inside solid–liquid hydrocyclones [12–16]. Generally it is considered that the following form describes tangential velocity distribution in the main flow:

$$u_\lambda r^n = C \tag{1}$$

where u_λ is the tangential velocity, r the radius coordinate, n the index to be experimentally correlated, normally falling between 0.5 and 1, and C is a constant.

For light dispersion hydrocyclones, Thew et al. [17] studied residence time distribution characteristics and gave axial velocity distribution. Wolbert et al. [18] introduced axial velocity correlation for small cone angle area as

$$\frac{u_{1z}}{u_{1zw}} = -3.33 + 12.0\frac{r_1}{R_{1z}} - 8.63\left(\frac{r_1}{R_{1z}}\right)^2 + 1.19\left(\frac{r_1}{R_{1z}}\right)^3 \tag{2}$$

where the subscripts "1" and "z" denote small cone angle area and axial direction, and r and z are coordinates in cylindrical coordinate system as shown in Fig. 2. R_{1z} represents the radius of hydrocyclone wall at axial level z_1 (seen in Fig. 3). u_{1zw} is the superficial axial velocity at axial level z_1, defined by:

$$u_{1zw} = \frac{Q}{\pi R_{1z}^2} \tag{2a}$$

where Q is the inlet flowrate.

Eq. (2) describes measured axial velocity in small cone angle areas of Thew type hydrocyclones. In a hydrocyclone different from Thew type, however, problems arise when we consider whether Eq. (2) holds true.

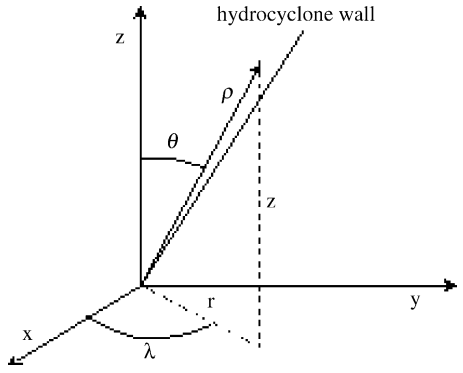

Fig. 2. Spherical coordinate system (ρ, θ, λ) and cylindrical coordinate system (r, λ, z).

Recently, ZHAO and MA [11] developed a theoretical algorithm for calculating migration probabilities of light dispersion hydrocyclones and by solving the momentum equation in spherical coordinate system (seen in Fig. 2) gave stream functions as

$$\varphi_1 = \sigma_1\gamma_1^2\left\{\left[K_1 - \ln\tan\left(\frac{\theta_1}{2}\right)\right]\sin^2\theta_1 - (1-\cos\theta_1)\right\} - D_1(1-\cos\theta_1) \quad (3)$$

and

$$\varphi_2 = \sigma_2\gamma_2^2\left\{\left[K_2 - \ln\tan\left(\frac{\theta_2}{2}\right)\right]\sin^2\theta_2 - (1-\cos\theta_2)\right\} - D_2(1-\cos\theta_2) \quad (4)$$

where φ is dimensionless stream function based on $Q/2\pi$, subscripts 1 and 2 represent small cone angle area and large cone angle area respectively, and γ is the dimensionless form of coordinate defined by $\gamma_1 = \rho_1/R_c$ and $\gamma_2 = \rho_2/R_c$. It should be noted that points (ρ_1, θ_1) and (ρ_2, θ_2) are measured from their respective origins defined by intersected points of extended line of hydrocyclone wall and central axis, that is, points O_1 and O_2 in Fig. 3.

K, D and σ in Eqs. (3) and (4) are integral coefficients and can be determined by:

$$K_1 = \frac{1}{1+\cos\alpha_1} + \ln\tan\left(\frac{\alpha_1}{2}\right) \quad (3a)$$

$$D_1 = \frac{1-F}{1-\cos\alpha_1} \quad (3b)$$

$$\sigma_1 = \frac{D_1}{\gamma_{1u}^2(1+\cos\theta_{1u})\ln[\tan(\alpha_1/2)/\tan(\theta_{1u}/2)]} \quad (3c)$$

$$K_2 = \frac{1}{1+\cos\alpha_2} + \ln\tan\left(\frac{\alpha_2}{2}\right) \quad (4a)$$

$$D_2 = \frac{1-F}{1-\cos\alpha_2} \quad (4b)$$

where α and F denote semi cone angle and split ratio (the ratio of the overflow flowrate to total inlet flowrate) respectively, $\gamma_{1u} = \rho_{1u}/R_{10}$, $\rho_{1u} = \sqrt{R_o^2 + z_{1u}^2}$, $\theta_{1u} = \arctan(R_o/z_{1u})$, and $z_{1u} = R_u/\tan\alpha_1$. Point (R_o, z_{1u}) (seen in Fig. 4) in cylindrical coordinate system corresponds to the point $\varphi_1 = 0$ when fluid immediately reaches underflow orifice.

In the same way, σ_2 can be determined by:

$$\sigma_2 = \frac{D_2}{\gamma_{2u}^2(1+\cos\theta_{2u})\ln[\tan(\alpha_2/2)/\tan(\theta_{2u}/2)]} \quad (4c)$$

where $\gamma_{2u} = \rho_{2u}/R_c$, $\rho_{2u} = \sqrt{R_{1m}^2 + z_{2u}^2}$, $\theta_{2u} = \arctan(R_{1m}/z_{2u})$, and $z_{2u} = R_c/\tan\alpha_2$. R_{1m}, z_{1u} and z_{2u} are all shown in Fig. 4.

Eqs. (3) and (4) can give stream function values at any points in the two cone areas. Then, velocity distributions can be deduced as

$$u_{1r}^* = -2\sigma_1\frac{1-\cos\theta_1}{\sin\theta_1} - \frac{D_1}{\gamma_1^2}\sin\theta_1 \quad (5)$$

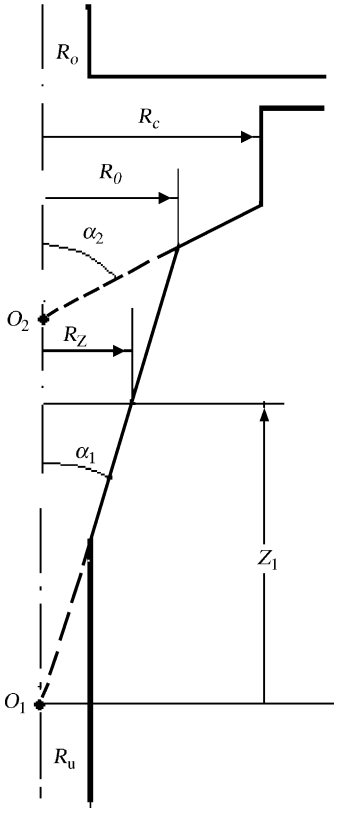

Fig. 3. Design parameters.

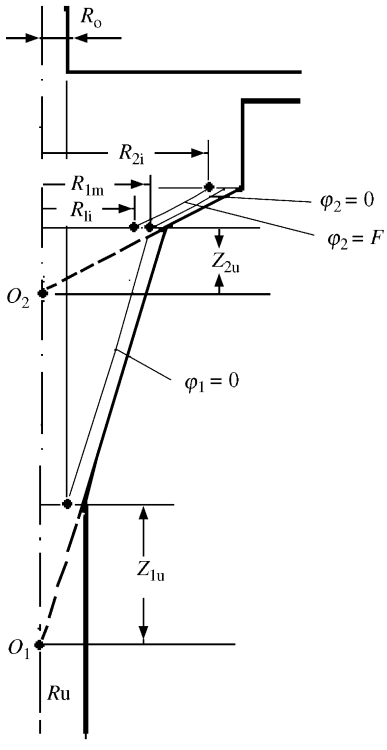

Fig. 4. Parameters for determining σ_1 and σ_2.

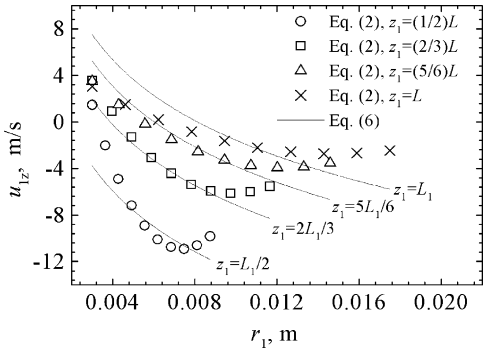

Fig. 5. Comparisons of axial velocities calculated by Eqs. (6) and (2).

$$u^*_{1z} = 2\sigma_1 \left[K_1 - 1 - \ln \tan\left(\frac{\theta_1}{2}\right)\right] - \frac{D_1}{\gamma_1^2} \cos\theta_1 \tag{6}$$

$$u^*_{1\lambda} = \frac{\sqrt{(V_1/\mathrm{vel}_1)^2 + 2\sigma_1[\varphi_1 + (1-F)]}}{\gamma_1 \sin\theta_1} \tag{7}$$

in the small cone-angle zone, and:

$$u^*_{2r} = -2\sigma_2 \frac{1-\cos\theta_2}{\sin\theta_2} - \frac{D_2}{\gamma_2^2} \sin\theta_2 \tag{8}$$

$$u^*_{2z} = 2\sigma_2 \left[K_2 - 1 - \ln \tan\left(\frac{\theta_2}{2}\right)\right] - \frac{D_2}{\gamma_2^2} \cos\theta_2 \tag{9}$$

$$u^*_{2\lambda} = \frac{\sqrt{(V_2/\mathrm{vel}_2)^2 + 2\sigma_2[\varphi_2 + (1-F)]}}{\gamma_2 \sin\theta_2} \tag{10}$$

in the large cone-angle zone respectively, where superscript * means dimensionless velocities based on $\mathrm{vel}_1 = Q/(2\pi R_0^2)$ in the small cone angle area and on $\mathrm{vel}_2 = Q/(2\pi R_c^2)$ in the large cone angle area. V_1 and V_2 are superficial maximum tangential velocities when fluid immediately enters small cone angle and large cone angle area respectively, and defined by $V_1 = \sqrt{-(\sigma_1 Q W_1/\pi R_0^2)}$ and $V_2 = \sqrt{-(\sigma_2 Q W_2/\pi R_c^2)}$. W_1 and W_2 in V_1 and V_2 definitions are superficial axial velocities, again when fluid immediately enters small and large cone angle areas respectively. They can be calculated by $W_1 = -(Q/\pi(R_0^2 - R_{1i}^2))$ and $W_2 = -(Q/\pi(R_c^2 - R_{2i}^2))$ where R_{1i} and R_{2i} correspond to the points $\varphi_1 = F$ and $\varphi_2 = F$ immediately at entries of small and large cone angle areas and are also shown in Fig. 4.

Through Eqs. (5)–(10), three velocity components at any points in two cone areas can be determined. Calculation according to ZHAO and MA's algorithm [11] will be complicated, but is very convenient because it is available for various hydrocyclones, rather than for Thew type only, whenever design parameters, operating conditions and fluid properties are given. Fig. 5 shows comparisons of calculated axial velocities in small cone angle area according to Eq. (6) and those according to Eq. (2). Calculations are carried out from $r_1 = R_o$ to $r_1 = R_{1z}$ where each $r_1 = R_{1z}$ corresponds to the point at hydrocyclone wall at each z_1 level. L_1 in Fig. 5 denotes the height of small cone angle area

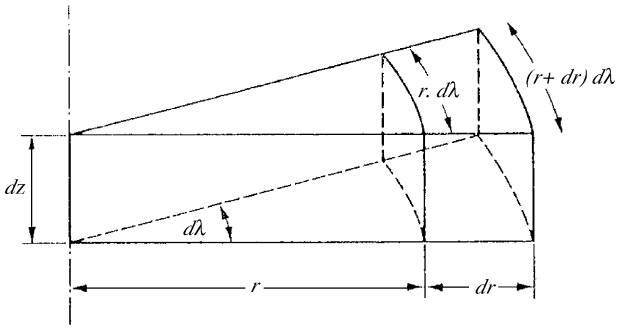

Fig. 6. Element of fluid in a rotating body.

given by $L_1 = R_0/\tan\alpha_1$. It can be seen that Eqs. (5)–(7) can give reasonable good predictions in the main flow except points near the wall where a laminar boundary layer exists.

2.2. Effective pressure drop

Consider a fluid element as shown in Fig. 6. Let the pressure at radius r be p and at radius $r+\mathrm{d}r$ be $p+(\mathrm{d}p/\mathrm{d}r)\,\mathrm{d}r$. Then net pressure (neglecting second order terms) in r direction $(p + (\mathrm{d}p/\mathrm{d}r)\,\mathrm{d}r)(r + \mathrm{d}r)\,\mathrm{d}\lambda\,\mathrm{d}z - pr\,\mathrm{d}\lambda\,\mathrm{d}z - 2(p + (1/2)\,\mathrm{d}p)\,\mathrm{d}r\,\mathrm{d}z \sin(\mathrm{d}\lambda/2)$ balances the centrifugal acceleration of the element $\rho(r + (1/2)\,\mathrm{d}r)\,\mathrm{d}\lambda\,\mathrm{d}r\,\mathrm{d}z\,u_\lambda^2/r + (1/2)\,\mathrm{d}r$.

Again neglecting second order term this becomes [12]:

$$\frac{\mathrm{d}p}{\mathrm{d}r} = \frac{\rho u_\lambda^2}{r} \tag{11}$$

Eq. (11) is the generalized relationship describing pressure–velocity relationship of a rotating fluid. It is of course available in calculating pressure variations in hydrocyclones.

Now velocity components can be calculated according to Eqs. (5)–(10). Take 30 mm Thew type hydrocyclone for example, calculated tangential velocities in small cone angle area are shown in Fig. 7. They can be well correlated in the form of Eq. (1) as shown in Table 1.

Now that tangential velocities in both cone areas can be calculated according to Eqs. (5)–(10) and correlated in the form of Eq. (1), we can take tangential velocity in the form of Eq. (1) into Eq. (11). Note that energy conversion from static to kinetic form happens across whole downward outer flow region from $r_2 = R_c$ to $r_2 = R_o$ (corresponding to points "o" and "w" in Fig. 8), and

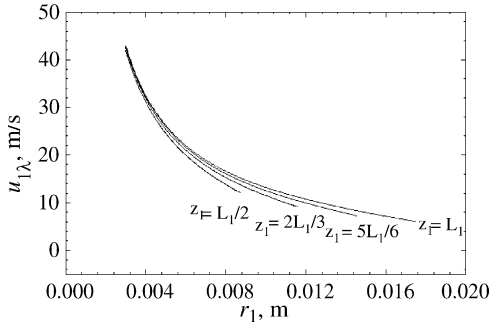

Fig. 7. Tangential velocity distributions.

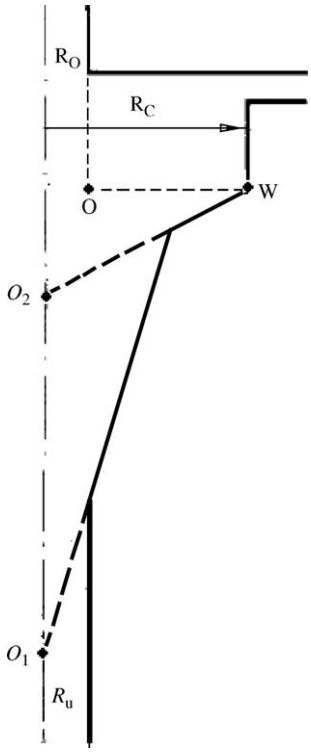

Fig. 8. integration region from point "w" to point "o".

integration in r direction should cover this region. This leads to:

$$\Delta p = p_{\mathrm{w}} - p_{\mathrm{o}} = \int_{R_{\mathrm{o}}}^{R_{\mathrm{c}}} \frac{\rho u_{2\lambda}^2}{r_2}\,\mathrm{d}r = \int_{R_{\mathrm{o}}}^{R_{\mathrm{c}}} \frac{\rho (C/r_2^n)^2}{r_2}\,\mathrm{d}r = C^2 \int_{R_{\mathrm{o}}}^{R_{\mathrm{c}}} \rho r_2^{-(2n+1)}\,\mathrm{d}r \tag{12}$$

$$\Delta p = \frac{\rho C^2}{2nR_{\mathrm{c}}^{2n}} \left[\left(\frac{R_{\mathrm{c}}}{R_{\mathrm{o}}} \right)^{2n} - 1 \right] \tag{12a}$$

Table 1
Correlated n and C in Eq. (1) for tangential velocity distributions

Axial level, z	n	C
$L_1/2$	0.352163	0.0977404
$2L_1/3$	0.364492	0.120813
$5L_1/6$	0.373569	0.140209
L_1	0.381381	0.158575

$$\Delta p = \frac{\rho u_{2\lambda,\mathrm{w}}^2}{2n} \left[\left(\frac{R_{\mathrm{c}}}{R_{\mathrm{o}}} \right)^{2n} - 1 \right] \tag{12b}$$

where coefficient C and index n can be obtained by correlating tangential velocity distributions calculated according to Eqs. (5)–(10), and $u_{2\lambda,\mathrm{w}} = C/R_{\mathrm{c}}^n$ is the tangential velocity near the wall, that is, the calculated tangential velocity at point "w" shown in Fig. 8.

Eq. (12a) or (12b) defines the pressure drop necessary for energy conversion from static to kinetic form. As has been explained in the introduction part, it denotes effective pressure drop in cone areas of hydrocyclones.

3. Experimental

3.1. Experimental procedure

Experimental setup was established to measure pressure drop in cone areas of light dispersion hydrocyclone, as shown in Fig. 9. Fluid was pumped from water tank to hydrocyclone. The flow rate entering hydrocyclone was adjusted by an adjusting valve and measured by a turboflowmeter. The physical properties of fluid were obtained according to the fluid temperature measured at hydrocyclone entry using a thermocouple. Another turboflowmeter was used to measure the flowrate of underflow stream, and by balancing the overall flowrates entering and leaving the hydrocyclone the overflow flowrate can be determined. Both underflow and overflow streams were led to water tank for recycling. Pressure was measured at three locations, i.e. "A",

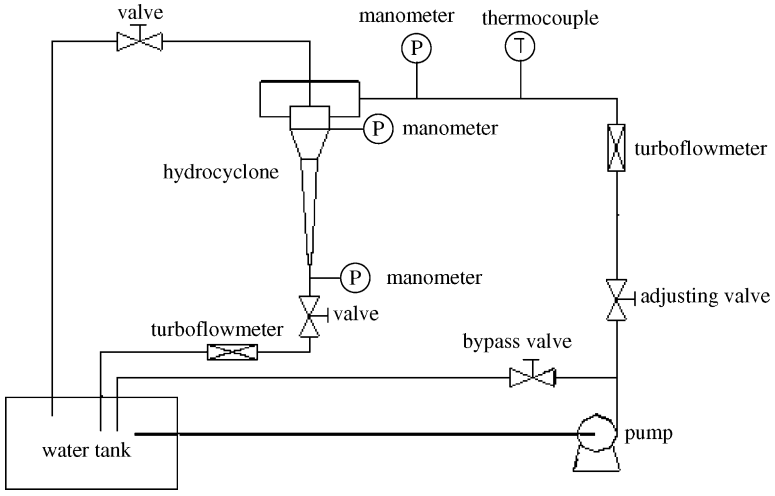

Fig. 9. Experimental setup for pressure drop measurement.

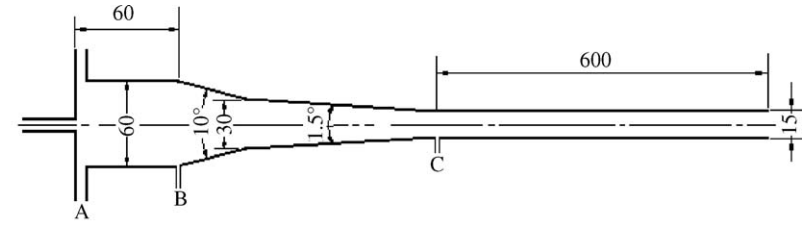

(a) Hydeocyclone Geometry

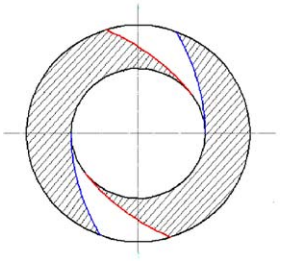

(b) twin tangential inlets arrangement

Fig. 10. Testing hydrocyclone.

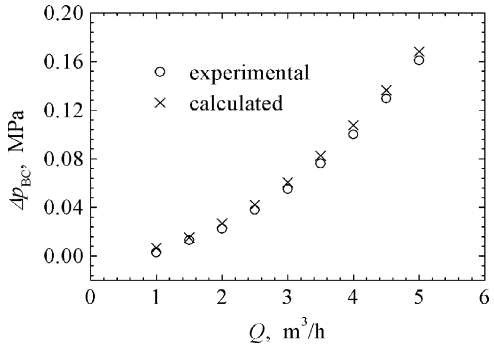

Fig. 11. Effective pressure drop vs. flowrate of hydrocyclone with cycloid inlets.

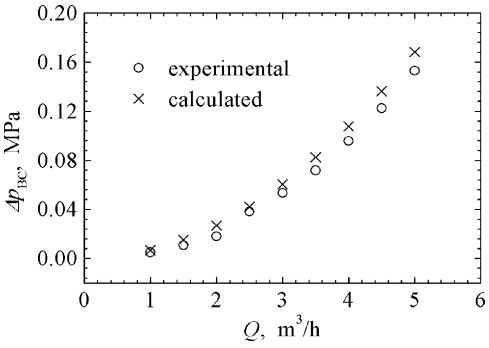

Fig. 12. Effective pressure drop vs flowrate of hydrocyclone with involute inlets.

"B" and "C", as shown in Fig. 10. Pressure data from manometers were all within the accuracy of ±0.001 MPa. By adjusting valves in underflow and overflow streams, split ratio.could be varied.

3.2. Hydrocyclone

Main design parameters of testing hydrocyclone are shown in Fig. 10a. There are twin inlets (Fig. 10b) leading fluid tangentially entering hydrocyclone. Inlet fluid channels are varied in terms of cycloid and involute forms with equivalent diameter of $0.35D_c$ (where D_c is the diameter of cylindrical section). Overflow diameter could be interchanged to be 6, 7, 8 or 9 mm. Inlet flowrate varied within the range of 1–5 m^3/h, while split ratio covered 0.5–16%.

4. Results and discussion

Figs. 11 and 12 show comparisons of measured and calculated effective pressure drop in conical section of hydrocyclone with cycloid and involute inlets respectively, at split ratio $F = 6\%$ and $R_o = 4$ mm. It is seen that calculated results are all in very good agreement with measured ones. In the range of flowrate tested, effective pressure drop can be well correlated to flowrate by $\Delta p_{BC} = -0.000816 - 0.00186Q + 0.00667Q^2$. The calculated results are more or less higher than the measured but differences between them can be neglected in a hydrocyclone design practice. Figs. 13 and 14 compare measured and calculated effective pressure drop versus split ratio of two

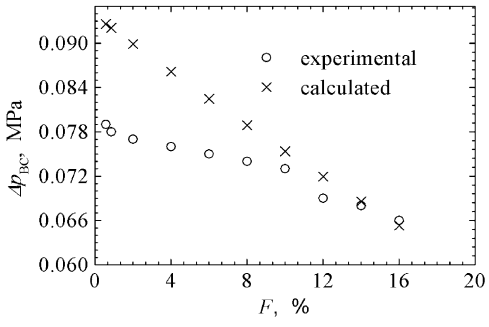

Fig. 13. Effective pressure drop vs. split ratio of hydrocyclone with cycloid inlets.

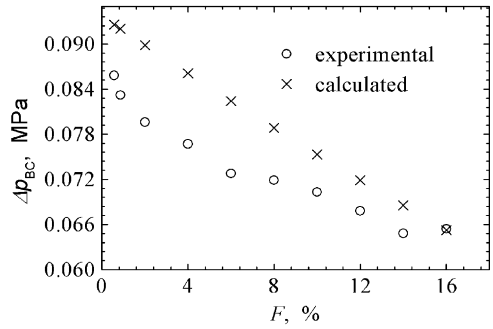

Fig. 14. Effective pressure drop vs split ratio of hydrocyclone with involute inlets.

inlet hydrocyclones at flow rate $Q = 3.5\ m^3/h$ and $R_o = 4$ mm. Effective pressure drop decreases with increase of split ratio. Differences between the calculated and measured pressure drop are clearly displayed in these figures, probably due to differences between ideal symmetric flow assumption in theoretical model and actual asymmetric flow during experiment. It is likely that the central axis of exchangeable overflow tube does not exactly superposed with hydrocyclone central axis, as shown in Fig. 15. In this case the fluid must adapt itself to the actual overflow orifice where upward inner flow spirals point to. This situation makes the actual diameter d_{o1} of upward inner flow body larger than the overflow tube diameter d_o and thus decrease the effective pressure drop in terms of Eq. (12), leading to lower pressure drop than predicted. The lower the split ratio, the more prominent the effect. When split ratio increases, the experimental pressure drop would be close to the predicted. Fig. 16 gives effective pressure drop variations with radius of overflow orifice at $Q = 3.5\ m^3/h$ and $F = 6\%$. Pressure drop increases with increase of overflow orifice radius. This phenomenon cannot be directly observed from Eq. (12) because increase of $u^2_{2\lambda,w}$ with overflow orifice radius R_o is not explicitly expressed. Again differences between experimental pressure drop and the predicted are clearly shown in Fig. 16. A tentative explanation can be made as follows: it would be more difficult for upward inner fluid spirals to point to smaller overflow orifice for a certain split ratio, and additional energy must be provided in the case of eccentric

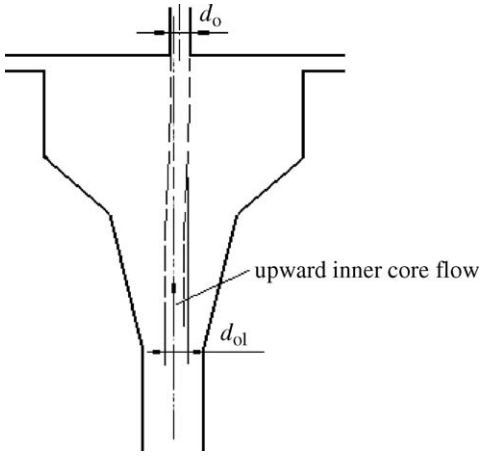

Fig. 15. Deviation of overflow central axis from hydrocyclone central axis.

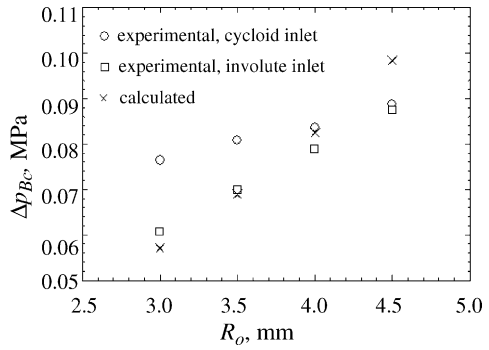

Fig. 16. Effective pressure drop vs. overflow orifice size.

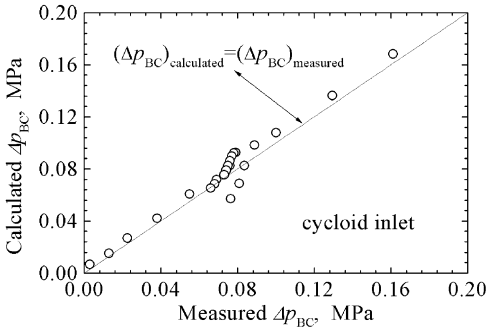

Fig. 17. Calculated effective pressure drop vs the measured data for hydrocyclone with cycloid inlets.

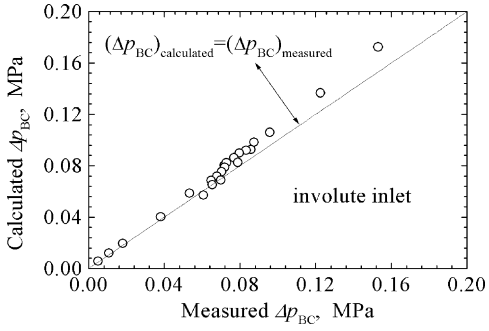

Fig. 18. Calculated effective pressure drop vs the measured for hydrocyclone with involute inlets.

installation of overflow orifice, resulting in higher experimental pressure drop than the predicted. As overflow diameter increase, this kind of difference would gradually disappear.

For a comprehensive comparison of calculated effective pressure drop with those measured, data from Figs. 11–14, and Fig. 16 can be incorporated into Figs. 17 and 18 for cycloid and involute inlets respectively. From theses Figures, it is very clear that though effective pressure drop data calculated according to the approach developed in present paper are more or less higher than the measured data they are on the whole in very good agreement with the measured results.

5. Concluding remarks

A theoretical approach has been established for calculating effective pressure drop of light dispersion hydrocyclones. It has

been verified that predicted results are on the whole in very good agreement with those measured. According to this approach, studies can be carried out on influences of design parameters on effective pressure drop, and these influences have been implicitly included in relationships of $u_{2\lambda,w}$ and n in Eq. (12) with design parameters.

Acknowledgement

This research was financially supported by the Natural Science Foundation Of Beijing Municipality, China (No. 8032006) and the National Natural Science Foundation of China (No. 50476035).

References

[1] D.A. Colman, M.T. Thew, D.R. Corney, Hydrocyclones for oil–water separation, in: Paper 11 Presented at International Conference on Hydrocyclones, Cambridge, UK, 1980, pp. 143–166.
[2] I.C. Smyth, M.T. Thew, P.S. Debenhan, D.A. Colman, Small-Scale experiments on hydrocyclones, in: Paper 14 Presented at International Conference on Hydrocyclones, Cambridge, UK, 1980, pp. 189–208.
[3] D.A. Colman, M.T. Thew, Correlation of separation results from light dispersion hydrocyclones, Chem. Eng. Res. Des. 61 (1983) 233–240.
[4] D.A. Colman, M.T. Thew, The concept of hydrocyclones for separating light dispersions and a comparison of field data with laboratory work, in: Paper F2 Presented at Second International Conference on Hydrocyclones, Bath, UK, 1984, pp. 217–232.
[5] K. Nezhati, M.T. Thew, Aspects of the performance and scaling of hydrocyclones for use with light dispersions, in: Paper G1 Presented at Third International Conference on Hydrocyclones, Oxford, UK, 1987, pp. 167–180.
[6] D.A. Flanlgan, J.E. Stolhand, E. Shimoda, et al., Use of low-shear pumps and hydrocyclones for improved performance in the cleanup of low-pressure water, SPE Prod. Eng. 7 (3) (1992) 295–300.
[7] D.A. Hadfield, S. Riibe, Hydrocyclones in large-scale marine oil spill cleanup, in: Proceedings of the 23rd Annual Offshore Technology Conference, OTC 6504, vol. 1, Houstin, May 6–9, 1991, pp. 39–48.
[8] M.F. Schubert, Advancements in liquid hydrocyclone separation systems, in: Proceedings of the 24th Annual Offshore Technology Conference, OTC 6869, vol. 1, Houston, May 4–7, 1992, pp. 497–506.
[9] G.A.B. Young, W.D. Wakley, et al., Oil–water separation using hydrocyclones: an experimental search for optimum dimensions, J. Pet. Sci. Eng. 11 (1994) 37–50.
[10] R.M. Martins, C.A.N. Dias, A.N. Feres, A theoretical-experimental method for analysis of hydrocyclones for treating oily waters. Hydrocyclone'96, in: D. Claxton, L. Svarovsky, M. Thew (Eds.), Proceedings of the Sixth International Conference on Hydrocyclones, Mechanical Engineering Publications Limited, Cambrigde, Bury St Edmunds, UK, 1996, pp. 333–344.
[11] Q.-G. ZHAO, C.-F. Ma, Theoretical predictions of migration probability of hydrocyclones separating light dispersions, Chin. J. Chem. Eng. 10 (2) (2002) 183–189.
[12] D. Bradley, The Hydrocyclone, Pergamon Press, London, 1965.
[13] W.W. Schwalbach, Three simple steps to hydrocyclone selection, Filtr. Sep. 25 (4) (1988) 264–266.
[14] J. Xu, Q. Luo, J. Qui, Studying the flow field in a hydrocyclone with no forced vortex, Filtr. Sep. (July/August) (1990) 276–278.
[15] P.M. Mikhaylov, A.A. Romenskiy, On calculation of flow dynamics in liquid cyclones, Fluid Mech. Soviet Res. 3 (1) (1974) 154–159.
[16] M.I.G. Bloor, D.B. Ingham, The flow in industrial cyclones, J. Fluid Mech. 178 (1987) 507–519.
[17] M.T. Thew, C.M. Wright, D.A. Colman, RTD characteristics of hydrocyclones for the separation of light dispersions, in: Proceedings of the Second International Conference on Hydrocyclones, Bath, England, 1984, pp. 163–176.
[18] D. Wolbert, B.-F. Ma, Y. Aurelle, Efficiency estimation of liquid–liquid hydrocyclones using trajectory analysis, AIChE J. 41 (6) (1995) 1395–1402.